Unraveling the differences of the reactivity of 3-methylthiophene and benzothiophene over bulk NiMoS catalysts using an experimental and kinetic modeling study

Alexandre Carvalho, Valentin Hetier, Julie Rousseau, Etienne Girard, Denis Uzio, Patrick Lacroix-Desmazes, Annie Pradel, Laurence Courthéoux, Sylvette Brunet

UNRAVELLING THE DIFFERENCES OF THE REACTIVITY OF 3-METHYLTHIOPHENE AND BENZOTHIOPHENE OVER BULK NiMoS CATALYSTS USING AN EXPERIMENTAL AND KINETIC MODELING STUDY

Alexandre Carvalho[1], Valentin Hetier[2], Julie Rousseau[1], Etienne Girard[3], Denis Uzio[3], Patrick Lacroix-Desmazes[2], Annie Pradel[2], Laurence Courthéoux[2], Sylvette Brunet[1]

[1]*Institut de Chimie des Milieux et Matériaux de Poitiers (IC2MP), Université de Poitiers, UMR 7285 CNRS, 4 rue Michel Brunet, TSA 71106, 86073 Poitiers, France*

[2]*ICGM, Univ Montpellier, CNRS, ENSCM, Montpellier, France*

[3] *IFPEN, Rond-point de l'échangeur de Solaize, BP3, 69360 Solaize, France*

*Corresponding author: email sylvette.brunet@univ-poitiers.fr (Sylvette Brunet)

Abstract

The reactivities of two model molecules, 3-methylthiophene (3MT) and benzothiophene (BT), representative of those contained in a FCC gasoline, was investigated over two Ni-promoted MoS_2 (NiMoS) bulk catalysts prepared according to two synthesis procedures, a metathesis-like one (NiMoS-M) and an innovative one including an in-situ Ni promotion (NiMoS-NG). The second procedure led to smaller NiMoS particles with a narrower size distribution and higher Ni promotion rate. Differences in the activity of the catalysts were observed for the transformation of 3MT and BT. BT was more reactive than 3MT over NiMoS-M whereas the reactivity of both sulfur molecules became similar over NiMoS-NG. The kinetic modeling indicated a higher adsorption constant of 3MT over NiMoS-NG than NiMoS-M and similar adsorption constant of BT on both catalysts. The results have been interpreted taking into account the differences of the catalyst properties in relation with the mechanisms involved in the transformation of both molecules.

Graphical abstract

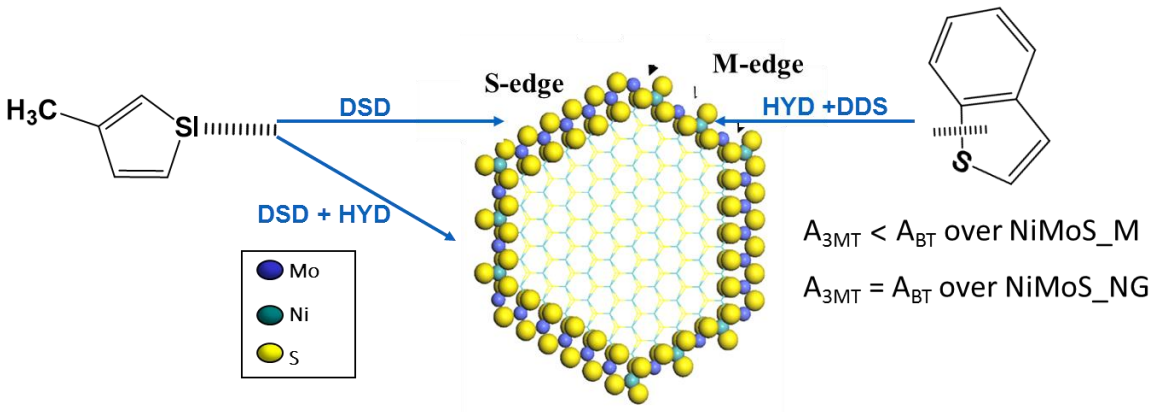

Highlights

- Influence of synthesis procedures for NiMoS catalyst properties
- Innovative synthesis of MoS_2 bulk catalysts with remarkable Ni promotion
- Strong difference in reactivity of 3-methylthiophene and benzothiophene
- Importance of coupled “experimental/kinetic modeling” studies
- Importance of adsorption/reaction mechanisms of sulfur molecules for the catalyst efficiency)

Keywords:

NiMoS bulk catalysts, metathesis, thiomolybdate reduction, in-situ Ni promotion, hydrodesulfurization, 3-methylthiophene, benzothiophene, kinetic modeling

1. Introduction

Worldwide growth of the global mobility of people and merchandises, along with industrial activity, have resulted in a severe increase in airborne pollutant concentration in the last decades. The production of cleaner fuels for on-road and off-road transportations is therefore a requirement, which will remain relevant until new energy sources take over the use of fossil resources. This stimulates research and innovations in hydrotreatment processes and heterogeneous catalysts. For example, the reduction of sulfur content in gasoline and diesel cuts through hydrodesulfurization (HDS) processes have become essential to meet present and future worldwide regulations (e.g., China V and US Tier 3 regulations impose a 10 ppm maximum of sulfur in gasoline since 2017)[1]. Moreover, the availability of metals resources is increasingly limited and becomes a new and important incentive to improve the efficiency of processes and catalysts. In order to meet the new specifications, to make hydrotreating processes more eco-efficient, and to address the metal resource issue, scientific breakthroughs are consequently highly needed to improve the performances of transition metal sulfide catalysts (activity, selectivity, stability over time) and their ease of utilization (activation, regeneration).

Conventional hydrotreating catalysts are based on transition metal sulfides (MoS_2) usually promoted by nickel or cobalt. The active phase is made of lamellar 2H MoS_2 nanostructures. Each Mo atom in the bulk of the crystalline structure is surrounded by six sulfur atoms in a trigonal prismatic arrangement. Active sites (uncoordinated surface atoms) are located at the edges of the slabs. The so-called S or M (for Sulfur and Metal) edges are also the preferential locations of the Co or Ni promoters, which drastically increase the catalytic activity [2-5].

Improvements of the catalytic performances could be achieved through a better control of the physico-chemical properties of the active phase such as size, shape and assembly (stacking) of

the Ni(Co)MoS slabs, surface properties (promotion degree) or electronic properties. This comes with developing new preparation protocols allowing a fine control at nanometer scale. Hydrotreatment catalysts are usually prepared by incipient wetness impregnation of metal precursor solutions on a porous carrier, usually transition alumina, followed by a sulfidation step [6,7]. Although significant improvements of such preparation methods (use of optimized supports, heteropolyanions (PolyOxoMetallate) as metallic precursors, addition of organic additives…) have been accomplished [28-12], catalytic performances seem to reach a plateau mainly due to the limit in metal loading which can be deposited in the porous volume of the support.

Unsupported (so called "bulk") Ni or Co promoted MoS_2 catalysts can represent an alternative to overcome these limitations, with the aim to maximize their activity per volume of reactor. Most of the studies on such unsupported catalysts reported the co-precipitation of mixed oxide phases followed by a sulfidation step [13-17]. Some other papers described the synthesis of MoS_2 based catalysts starting from thio precursors under various conditions [18-26]. Whatever the precursor, the synthesis of promoted MoS_2 catalysts is usually performed in several steps, either with the formation of MoS_2 phase followed by the promotion by cobalt or nickel or else with the formation of (Co)NiMoO_x followed by a sulfidation step [19,27]. A fast and direct metathesis-like synthesis of (Co)NiMoS bulk catalyst has also been described [28,29]. This instantaneous reaction between equimolar solutions of ammonium thiomolybdate and nickel nitrate easily proceeds in water without hydrothermal treatment.

In the present paper, two bulk NiMoS catalysts were prepared using two different synthesis procedures, namely metathesis (M) and nucleation/growth (NG) partly inspired from Bezverkhy work [30]. The hydrodesulfurization (HDS) of two sulfur molecules, 3-methylthiophene (3MT) and benzothiophene (BT), was then studied in the presence of the previously prepared bulk NiMoS catalysts and modelled using a kinetic model based on a

Langmuir-Hinshelwood formalism [31]. In this case, the objective was to deepen the knowledge of the transformation of 3MT and BT molecules representative of FCC gasoline cuts by coupling experimental and theoretical approaches.

2. Experimental

2.1 Chemicals

3-methylthiophene (98% purity), benzothiophene (95% purity), n-heptane (> 99% purity), sodium molybdate dihydrate $Na_2MoO_4.2H_2O$ (>99.5%), nickel nitrate $Ni(NO_3)_2.6H_2O$ (99.99%) and ethanol were purchased from Sigma-Aldrich (Sigma Aldrich, St. Louis, MO, USA) and used as such without any further purification. Pure hydrogen sulfide (H_2S) and hydrogen sulfide in mixture (1 vol%) with H_2 were purchased from Air Liquide (Air Liquide, Paris, France) and H_2 (5 vol %)/Ar (95 vol %) was provided by Linde gas (Linde, Dublin, Ireland).

2.2 NiMoS bulk catalyst preparations

Two synthesis processes were used to prepare the NiMoS catalysts, a first one, hereafter called metathesis (M) and a second one, hereafter called nucleation growth (NG). Ammonium tetrathiomolybdate, $(NH_4)_2MoS_4$ was used as the molybdenum precursor in the two processes. It was synthesized according to the procedure described by McDonald et al. [32].

2.2.1 Metathesis process (M)

This process, first proposed by Genuit [28], results from a straightforward and fast reaction between equimolar solutions of ammonium tetrathiomolybdate and nickel nitrate according to:

$$(NH_4)_2MoS_4 + Ni(NO_3)_2.6\ H_2O \rightarrow NiMoS_4 + 2\ NH_4NO_3 + 6\ H_2O \qquad \text{(Equation 1)}$$

In our case, $(NH_4)_2MoS_4$ (4 mmol) and $Ni(NO_3)_2 \cdot 6H_2O$ (4 mmol) were separately dissolved in 40 mL of pure H_2O. The two solutions were then mixed with gentle magnetic stirring for 30 s, in air at room temperature. The reaction mixture was then stored for 12 h at room temperature and the particles were separated by centrifugation (40,000 rpm, 4 h) using a Beckman Coulter Optima XPN ultracentrifuge with a 45 TI rotor and 70 mL PC tubes. Three washings with 80 mL of water were performed (centrifugation at 40,000 rpm, 4 h), followed by a final washing step with 80 mL of ethanol. The particles were finally recovered by centrifugation (20,000 rpm, 4 h) in 94 mL polypropylene tubes. The product was then dried under primary vacuum for 12 h at room temperature. Finally, the powder was heated under hydrogen (5% in argon) from room temperature to 320°C at 5°C.min^{-1}, held 2 h at 320°C, and cooled down to room temperature at the same rate under argon. The catalyst, labelled NiMoS-M, was stored under vacuum before use.

2.2.2 Nucleation growth method (NG)

The NG method is based upon a reduction of ammonium tetrathiomolybdate by hydrazine at 90°C according to the theoretical equation [33]:

$$(NH_4)_2MoS_4 + ½\ N_2H_4 \rightarrow MoS_2 + ½\ N_2 + (NH_4)_2S + H_2S \qquad \text{(Equation 2)}$$

And followed by the addition of nickel nitrate in a Ni/(Ni+Mo) molar ratio of 0.3. This ratio corresponds to the maximum catalytic activity for HDS reactions using NiMoS catalysts [10].

The experimental procedure was as follows: $(NH_4)_2MoS_4$ (4 mmol, 1 eq) was dissolved in 40 ml of ultrapure water and introduced into a three-necked flask. The reducing agent, hydrazine (40 mmol, 10 eq, 50-60% in water), was then added and the mixture was degassed by bubbling argon for 30 min in order to remove dissolved oxygen. At this stage, in order to prepare the later addition of nickel nitrate and to prevent a precipitation of $Ni(OH)_2$, the pH was adjusted to 7 by addition of hydrochloric acid (HCl, circa 3 mL). The bubbling of argon

was then replaced by a flow of hydrogen sulfide and the reaction medium was placed in an oil bath previously heated to 90°C. The progress of the reduction reaction, via the remaining amount of MoS_4^{2-}, was followed by UV-visible spectroscopy. The Ni solution (1.6 mmol, 0.4 eq of $Ni(NO_3)_2$ dissolved in 8 ml of ultrapure water) was introduced dropwise only after complete disappearance of MoS_4^{2-}, a necessary precaution to avoid an unwanted metathesis reaction between nickel nitrate and residual unreduced MoS_4^{2-}. When the addition of nickel was complete, the reaction medium was stirred for an additional 2 hours at 90°C under H_2S bubbling.

The particles were then separated by centrifugation (20,000 rpm) using a Beckman Coulter Optima XPN ultracentrifuge with a 45 TI rotor and 94 mL PP tubes. Three washings with 80 mL of water were performed, followed by a final washing step with 80 mL of ethanol. The product was then dried under primary vacuum for 12 h at room temperature. The sample was heated under 5% hydrogen in argon from room temperature to 350°C at 5°C.min^{-1}, held 2 h at 350°C, and cooled down to room temperature at the same rate under Ar. The catalyst, labelled NiMoS-NG, was stored under vacuum before use.

2.3 Characterizations

Specific surface areas were determined by nitrogen adsorption–desorption using a Micromeritics tristar apparatus after degassing at 120°C overnight (Micromeritics, Norcross, GA, USA). Elemental analysis (sulphur amount) was carried out using an Elementar Vario Micro Cube (Elementar, Langenselbold, Germany) while the molybdenum and nickel amounts were measured by inductively coupled plasma mass spectrometry (ICP-MS) using a SPECTRO ARCOS ICP-AOS analyzer (SPECTRO Analytical Instruments, Kleve, Germany). X-ray powder diffraction (XRD) patterns were recorded with a Malvern Panalytical X'pert PRO X-ray diffractometer by using Cu radiation (λ = 1.5406 Å) (Malvern Panalytical, Royston, U.K.). A JEOL JEM 2100LaB6 (JEOL, Tokyo, Japan) transmission

electron microscope (TEM) was used to characterize the MoS_2 phase and more precisely, the length and stacking distribution of the slabs.

XPS spectra were recorded using a KRATOS AXIS supra-spectrometer (Kratos Analytical, Manchester, U.K.) equipped with an aluminium monochromatic source (hν = 1486.6 eV). Before analysis, catalysts were treated at 400°C during 10 h by a mixing of H_2S (10 mol. %)/H_2 at atmospheric pressure and stored in Schlenk under Ar to avoid oxidation resulting in the formation of sulfates at the surface. The recorded spectra were analyzed using a CasaXPS software. The deconvolution of S 2p, Ni 2p and Mo 3d signals were carried out with respect to the appropriate standard samples (supported oxide and sulfided monometallic catalysts). The calibration was made with the peak of contamination carbon at 284.6 eV. For each catalyst, the metal and sulfur peaks were identified according to their binding energies [34,35]. The elemental surface composition of the catalysts, and therefore, the sulfur/metal atomic ratio (S/Me) and the active phase formation were determined from the area of the metal and sulfur peaks (the uncertainty of the values is around 20%)

2.4 Reaction conditions and analysis

Prior to the hydrodesulfurization (HDS) reactions, the catalysts were treated in situ by a feed containing 10 mol% H_2S in H_2 at atmospheric pressure and at 400°C for 14 h. The HDS of 3MT and BT were performed in a fixed bed micro-reactor under a total pressure of 2.0 MPa, with a ratio of H_2/liquid feed equal to 360 NL/L and a reaction temperature of 250°C. The thiophenic feeds (corresponding to 1000 ppmS) (0.3 wt% of 3MT or 0.42 wt% of BT) in n-heptane were injected in the reactor by a HPLC Gilson pump (307 series, pump's head volume: 5.0 cm^3). Table 1 shows the partial pressures of the different compounds for the sulfidation step and the transformation of different feeds. The solvent n-heptane was not converted under the applied experimental conditions. No catalyst deactivation within the duration of the test was observed for all the experiments.

As described in previous works [31,36], the feed and the products were injected on-line by means of an automatic sampling valve into a Varian gas chromatograph equipped with a PONA capillary column and a flame ionization detector. The contact time is defined as the ratio between the total mass flow rate of feed and the mass of catalyst. The catalytic activity (a) was calculated at isoconversion (30%) in a differential regime according to the following equation:

$$a = \ln\left(\frac{1}{1 - X_i}\right).\frac{F}{m_{cat}}$$

where F is the molar flow of the reactant in mmol/h, m_{cat} is the mass of catalyst in g and X_i is the reactant conversion (i = 3MT and BT). The activity per active molybdenum atom (those located in the edges and corners of the slabs) is defined as followed: $a_{Mo} = a.M_{Mo}/(m_{Mo}.D.6.023.10^{23})$ with a: activity in mmol/h/g, M_{Mo} : molar mass of molybdenum, m_{Mo}: mass of molybdenum in wt% determined by ICP, D : dispersion determined from TEM experiments where $D = \frac{\text{Mo edges+corner}}{\text{Mo total}} = \frac{\sum_i 6n_i - 6}{\sum_i 3n_i^2 - 3n_i + 1}$ with n_i : number of Mo atoms along one side of a MoS_2 slab determined from its length and i being the total number of slabs [39].

2.5 Kinetic modeling

The objective was to determine the kinetic and adsorption constants of the transformation of the two sulfur molecules, thus making it possible to explain the differences in reactivity of the NiMoS catalysts prepared according to the two synthesis methods. For this, it was chosen to use an experimental approach coupled with a theoretical approach, which allowed both to acquire data and to use them to calculate the different constants using the ReactOp kinetic software. For this, the different kinetic equations were written according to the reaction scheme previously established for the transformation of the two sulfur molecules.

The theoretical approach based on the Langmuir-Hinshelwood formalism was developed in a previous work [31] using ReactOp software®. In this kinetic model, it is assumed a

competitive adsorption over one type of active sites of H_2 and H_2S with heterolytic dissociations. The rate determining step is the first hydrogen addition [31,37,38] on the aromatic ring or double bond for BT and 3MT . The reaction schemes for the transformation of 3MT and BT compounds are given in Scheme 1 and Scheme 2, respectively. The transformation of 3MT, shown in Scheme 1, involves two consecutive reactions: C-S bond rupture to produce pentenes (HDS) followed by their hydrogenation to produce isopentane (HYD).

The two R_1 and R_2 consecutive reactions are

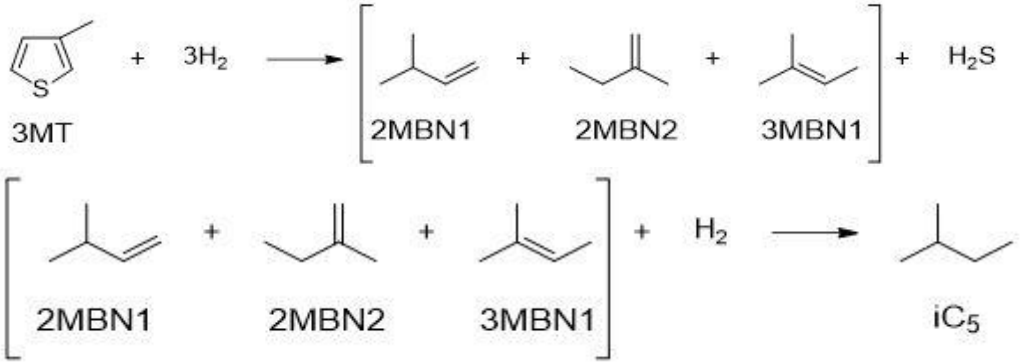

The corresponding rate equations, r_1 and r_2, are as follows:

$$r_1 = k_1 . e^{-\frac{Ea}{RT}} \frac{K_{3MT} P_{3MT} \sqrt{K_{H_2S} P_{H_2S}} \sqrt{\frac{P_{H_2S}}{K_S P_{H_2}}}}{\left(1 + K_{3MT} P_{3MT)} + \frac{P_{H_2S}}{K_S P_{H_2}} + \frac{K_{H_2} P_{H_2} \sqrt{\frac{P_{H_2S}}{K_S P_{H_2}}}}{\sqrt{K_{H_2S} P_{H_2S}}} + \sqrt{K_{H_2S} P_{H_2S}} \sqrt{\frac{P_{H_2S}}{K_S P_{H_2}}}\right)^2}$$

$$r_2 = k_2 . e^{-\frac{Ea}{RT}} \frac{K_{PN} P_{PN} \sqrt{K_{H_2S} P_{H_2S}} \sqrt{\frac{P_{H_2S}}{K_S P_{H_2}}}}{\left(1 + K_{PN} P_{PN} + \frac{P_{H_2S}}{K_S P_{H_2}} + \frac{K_{H_2} P_{H_2} \sqrt{\frac{P_{H_2S}}{K_S P_{H_2}}}}{\sqrt{K_{H_2S} P_{H_2S}}} + \sqrt{K_{H_2S} P_{H_2S}} \sqrt{\frac{P_{H_2S}}{K_S P_{H_2}}}\right)^2}$$

The transformation of BT can follow two pathways: In the first one, the BT transformation occurs through the two R_3 and R_4 consecutive reactions with a first HYD of BT into dihydrobenzothiophene (DHBT) followed by HDS of DHBT into ethylbenzene (EB):

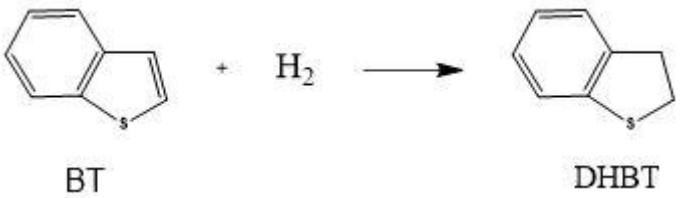

R_3

R_4

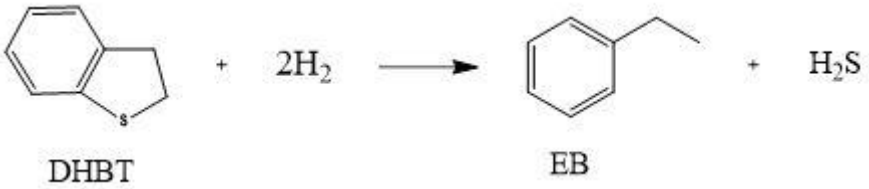

In the second pathway, ethylbenzene is directly formed from BT (DDS: Direct Desulfurization), according to reaction R_5:

R_5

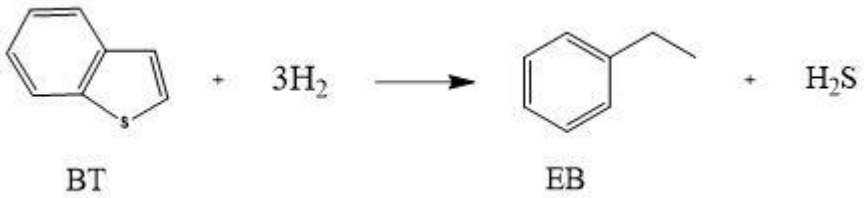

On the whole, the corresponding equation rates, r_3, r_4 and r_5, are as follows:

$$r_3 = k_3 . e^{-\frac{Ea}{RT}} \frac{K_{BT} P_{BT} \sqrt{K_{H_2S} P_{H_2S}} \sqrt{\frac{P_{H_2S}}{K_S P_{H_2}}}}{\left(1 + K_{BT} P_{BT} + \frac{P_{H_2S}}{K_S P_{H_2}} + \frac{K_{H_2} P_{H_2} \sqrt{\frac{P_{H_2S}}{K_S P_{H_2}}}}{\sqrt{K_{H_2S} P_{H_2S}}} + \sqrt{K_{H_2S} P_{H_2S}} \sqrt{\frac{P_{H_2S}}{K_S P_{H_2}}}\right)^2}$$

$$r_4 = k_4 . e^{-\frac{Ea}{RT}} \frac{K_{DHTB} P_{DHTB} \sqrt{K_{H_2S} P_{H_2S}} \sqrt{\frac{P_{H_2S}}{K_S P_{H_2}}}}{\left(1 + K_{DHTB} P_{DHTB} + \frac{P_{H_2S}}{K_S P_{H_2}} + \frac{K_{H_2} P_{H_2} \sqrt{\frac{P_{H_2S}}{K_S P_{H_2}}}}{\sqrt{K_{H_2S} P_{H_2S}}} + \sqrt{K_{H_2S} P_{H_2S}} \sqrt{\frac{P_{H_2S}}{K_S P_{H_2}}}\right)^2}$$

$$r_5 = k_3 . e^{-\frac{Ea}{RT}} \frac{K_{BT} P_{BT} \sqrt{K_{H_2S} P_{H_2S}} \sqrt{\frac{P_{H_2S}}{K_S P_{H_2}}}}{\left(1 + K_{BT} P_{BT} + \frac{P_{H_2S}}{K_S P_{H_2}} + \frac{K_{H_2} P_{H_2} \sqrt{\frac{P_{H_2S}}{K_S P_{H_2}}}}{\sqrt{K_{H_2S} P_{H_2S}}} + \sqrt{K_{H_2S} P_{H_2S}} \sqrt{\frac{P_{H_2S}}{K_S P_{H_2}}}\right)^2}$$

3 Results and discussion

3.1 Characterization of NiMoS bulk catalysts

NiMoS bulk catalysts prepared by metathesis (M) and nucleation growth (NG) were characterized after thermal treatment in a reductive atmosphere (5%H_2/95%Ar). Results of elemental analysis are given in Table 2. The amount of nickel is higher in NiMoS-M (17.6 wt.%) than in NiMoS-NG (8.9 wt.%), which corresponds to a Ni/(Ni+Mo) molar ratio of 0.45 and 0.3, respectively. These values are very close to the expected ones (0.5 for NiMoS-M since the synthesis proceeds by an equimolar reaction between Mo and Ni, and 0.3 for NiMoS-NG.

The N_2 adsorption–desorption isotherm curves for the NiMoS-M and NiMoS-NG compounds, shown in Figure 1, are similar and characteristic of inter-particle capillary condensation (type II according to IUPAC classification). The specific surface area is slightly higher (41 $m^2 \cdot g^{-1}$) for the NiMoS-NG compared to NiMoS-M (31 $m^2 \cdot g^{-1}$) (Table 2). These specific surface areas are higher than those reported by Fuentes *and al* and Fontaine *and al* [18,21] 18 $m^2 g^{-1}$ and 14

m^2g^{-1}, respectively. It may be understood on the basis of the different synthesis procedures used to prepare the catalysts. Indeed, our procedure is based upon a complete dissolution of tetrathiomolybdate in water while Fuentes and Fontaine's procedures comprise the preparation of a suspension of solid tetrathiomolybdate particles in acetone, with a further impregnation of the particles by nickel. Working at the molecular level as done in our procedure might favor the preparation of smaller particles and thus larger specific surface areas. The X-ray diffraction patterns of NiMoS-M and NiMoS-NG, shown in Figure 2, are similar with broad peaks characteristic of a poor crystallized MoS_2 structure. Additional diffraction peaks assigned to the presence of nickel sulfide NiS are also observed, a finding already reported in literature [40-42].

The size of the MoS_2 particles, estimated using the Scherrer formula, was found to be around 3.3 nm for NiMoS-M and 2.6 nm for NiMoS-NG (Table 3), which is consistent with the results from N_2 adsorption-desorption experiments, i.e. a higher specific surface area of NiMoS-NG compared to NiMoS-M (Table 2).

TEM images at macroscopic and microscopic scales of NiMoS-M and NiMoS-NG are shown in Figure 3. At macroscopic scale, a difference of morphology was observed between these two samples : a compact geometric grains whose size varies from 500 nm to several microns on a side for NiMoS_M (Figure 3a) instead a form of balls 20 to 50 nm in diameter for NiMoS_NG (Figure 3b). The image analysis (Figure 3c and Figure 3d) helped in determining the distributions of slabs depending upon their length (Figure 4) and stacking (Figure 5). Data are given in Table 3. The average stacking is ~4 and rather low for bulk catalysts. Reported values are usually higher than 5 [19,29,33]. The average length of the slabs is short especially for NiMoS-NG: 2.5 nm, compared to 3.7 nm for NiMoS-M, these values being very close to those reported above for XRD experiments. Moreover, the higher standard deviation for NiMoS-M (1.7 nm compared to 1.0 for NiMoS-NG) and thus the presence of some longer

slabs (10 – 11 nm) indicates a larger distribution in length. The dispersion D, which corresponds to the fraction of $Mo_{edges+corner}$ to the total amount of Mo, is larger for NiMoS-NG (36%) than for NiMoS-M (25%), a direct consequence of shorter average length of slabs for NiMoS-NG as compared to NiMoS-M.

X-ray photoelectron spectroscopy (XPS) was used to characterize NiMoS-M and NiMoS-NG catalysts. The decomposition of Mo 3d, S 2p and Ni 2p XPS spectra, shown in Figures 6, 7 and 8 respectively, revealed the co-existence of MoS_2, NiMoS, NiS and NiO phases. Indeed, the various MoS_2 (Mo 3d5/2 BE = 229,3 eV; S 2p3/2 BE = 162,2 eV), NiS (Ni 2p3/2 BE = 853,2 eV), NiO (Ni 2p3/2 BE = 856,1 eV) and mixed phase Ni-Mo-S (Ni 2p3/2 BE = 854,3 eV) species were well identified. Results from quantitative analysis of XPS spectra are given in Table 4. They confirmed the formation of MoS_2 phase (S/Mo ratio = 2.3 and 2.1) in a large amount, similar for the two catalysts (80% for NiMoS-M and 82% for NiMoS-NG). Owing to the large uncertainty (20%), the Ni/(Ni+Mo) atomic ratios values, 0.29 for NiMoS-NG and 0.39 for NiMoS-M, agree with the amount of nickel found by elemental analysis of the powders (0.3 and 0.45, respectively). These values are close to that of conventional $NiMo/Al_2O_3$ catalysts used in hydrotreament processes [10]. However, the chemical forms of Ni are not the same in the two catalysts. If the amount of Ni oxide phases is roughly the same for the two catalysts, a larger amount of NiS is found in NiMoS-M (28% compared to 9% for NiMoS-NG)) while the opposite is found for the mixed NiMoS phase. In both cases, large amounts of mixed Ni-Mo-S phase were formed. Yet, it is larger and particularly remarkable for NiMoS-NG (80% compared to 57% for NiMoS-M).

The physicochemical characterizations of the two catalysts lead to the following conclusions:

In the case of NiMoS-M, an almost instantaneous uncontrolled precipitation occurred. On the other hand, NiMoS-NG catalysts were synthesized through a slower process, i.e. a reduction of ammonium thiomolybdate, which favored the formation of many nuclei previous to

growth. Compared to NiMoS-M particles, the obtained particles were slightly smaller with a narrower distribution in size. They showed slightly higher specific surface area and dispersion. Moreover, the innovative way to introduce the promotor in the case of the NG procedure, i.e. directly after the disappearance of the MoS_4^{2-} species in the liquid phase, appeared to be a very effective way leading to a remarkable promotion.

3.2 HDS of the sulfur model compounds 3MT and BT

The reactivity of 3MT and BT, two sulfur model compounds representative of a FCC gasoline cut, over the two previously prepared NiMoS bulk catalysts was then investigated. Results of the study are reported in Figures 9-13 and Tables 5 and 6.

An increase of the conversion of 3MT and BT with the contact time was noticed for both catalysts, as shown in Figure 9a and Figure 11 respectively. For a given contact time, the conversion of 3MT and BT was higher for the NiMoS-NG. Thus, a conversion of 3MT of 17% for NiMoS-M (respectively 40% for NiMoS-NG) and a conversion of BT of 20% (45%) were measured at a contact time of 1h. For the two NiMoS-M and NiMoS-NG catalysts, the main products of the 3MT transformation were pentenes with isopentanes as secondary products as shown in Figure 9b. However, the ratio between the two products depended upon the catalysts as shown in Figure 10. Indeed, the ratio between isopentane/pentene was higher and increased linearly when the catalyst was NiMoS-M. This means that the hydrogenating function is more pronounced over NiMoS-M than over NiMoS-NG. Conversely, whatever the catalyst used, no difference in the product yields for BT transformation was observed. In both cases, ethylbenzene (EB) was the main product while dihydrobenzothiophene was formed in small amount as shown in Figure 12. The ratio between EB and DHBT was the same whatever the BT conversion and the catalyst, as shown in Figure 13. The catalyst activities of NiMoS-M and NiMoS-NG calculated at isoconversion (30%) for the transformation of 3MT and BT are given in table 5 and 6 respectively. In presence of NiMoS-M, BT was more

reactive than 3MT as classically reported in the literature [31,43,44]. On the other hand, the two sulfur compounds presented the same reactivity in presence of NiMoS-NG. The activity per gram of NiMoS-NG for the transformation of 3MT was doubled versus that of NiMoS-M whereas it was similar for the transformation of BT. The activity per molybdenum atom located in the corners and the edges (respectively reported Table 5 and Table 6 for the transformation of 3MT and BT) was also considered. In the case of the transformation of 3MT, the activity per molybdenum atom is slightly higher for NiMoS-NG as compared to NiMoS-M. Conversely, its activity per molybdenum atom is slightly lower for the transformation of BT. To explain the different performances of NiMoS-M and NiMoS-NG catalysts for the transformation of 3MT and BT, kinetic and adsorption constants were calculated using a kinetic model previously established in the presence of a commercial $CoMo/Al_2O_3$ catalyst [31] and on the basis of their respective reaction schemes described above (section 2.5).

The kinetic parameters (for the hydrodesulfurization and hydrogenation reactions) and the adsorption constants calculated from the model are reported in Table 5 and Table 6 for the transformation of 3MT and BT respectively. Good fits of the experimental data got during the transformation of 3MT and BT in presence of either NiMoS-M or NiMoS-NG were obtained, as shown in Figure 9 (conversion and product distribution for 3MT), Figure 11 (BT conversion) and Figure 12 (product distribution for BT). The adsorption constant of 3MT is higher in presence of NiMoS-NG than in presence of NiMoS-M, whereas the nature of the catalyst has hardly any effect on the adsorption constant of BT. It is consistent with the trends in the activity calculated from the experimental results.

To get some insight in the origin of the different reactivity of the two sulfur molecules 3MT and BT over NiMoS-M and NiMoS-NG, it is interesting to consider the different nature of the two model compounds.

It can be considered that 3MT will adsorb over the catalyst via σ bonding (perpendicular) by the sulfur atom [45,46] while BT will undergo a π bonding (flat) by the aromatic ring [47]. The transformation pathways of the two compounds are thus different. The transformation of 3MT occurs via the so called DDS route with the direct rupture of C-S bonds, which implies active sites located on both S-edges and M-edges of MoS_2 slabs. On the other hand, BT follows the hydrogenation route leading to DHBT as intermediate, which is expected to occur mainly on the M-edges.

As shown in Table 5, the activity of NiMoS-NG per gram of compound is twice higher than that of NiMoS-M for the transformation of 3MT and 3MT adsorption constant is larger in presence of NiMoS-NG. This result is consistent with the physicochemical characteristics of the catalysts, which indicated a larger number of active sites with a better promotion for NiMoS-NG and therefore, probably improved electronic properties of the sites leading to a stronger adsorption of 3MT.

The situation is different for the transformation of BT. It is not affected by the nature of both catalysts. Indeed, as shown in Table 6, the catalytic activity and adsorption constants are similar whether NiMoS-M or NiMoS-NG is used. In this case, as stated above, the transformation occurs on the M-edges alone. Therefore, fewer active sites are involved during BT transformation compared to 3MT one. Moreover, the size of BT and its flat adsorption over the catalysts are detrimental to the accessibility to the active sites. On the whole, while the improved characteristics of NiMoS-NG helped in the transformation of 3MT when most sites are accessible, they are ineffective for BT transformation owing to a large steric hindrance.

On the whole, this clearly shows that the characteristics of a bulk catalyst, either the number or properties of the active sites, which depend strongly on the synthesis procedure, might have a strong influence in the transformation of sulfur molecules, as shown in the case

of 3MT. On the other hand, such situation is not universal as shown by the absence of effect on BT molecule. This evidenced the difficulty to define a bulk catalyst that would have ideal properties to optimize the transformation of different families of sulfur molecules involving different transformation mechanisms.

4 Conclusion

.

In conclusion, two NiMoS bulk catalysts were first prepared using two different procedures, i.e. a metathesis-like procedure and an innovative way including a reduction step of a thiomolybdate followed by a step of in-situ Ni promotion. An almost instantaneous uncontrolled precipitation occurred in the first procedure while a slower reduction process characterized the second. As a result, more homogeneous, smaller particles with shorter lengths of the slabs, slightly higher specific surface area and larger dispersion was obtained in the latter procedure. Moreover, the Ni-promotion in the liquid phase just after the reduction step, appeared to be a very effective way leading to a remarkable promotion, higher than the promotion achieved in the case of the metathesis-like procedure. On the whole, all characteristics pointed for a more effective catalyst in the case of NiMoS-NG, which had to be further checked by a series of catalytic tests.

The study of the transformation of two model sulfur molecules, 3MT and BT, over the two catalysts, NiMoS-M and NiMoS-NG, coupled to a kinetic modeling study was then carried out and helped in unraveling their difference in reactivity. Indeed, the reactivity of BT was higher than that of 3MT over NiMoS-M but similar over NiMos-NG. Meanwhile, the reactivity of 3MT was doubled over NiMoS-NG compared to NiMoS-M. In the same way, hardly any change in the adsorption constant of BT over either NiMoS-M or NiMoS-NG was observed, whereas the adsorption constant of 3MT showed a clear increase over NiMoS-NG.

These differences can be attributed to the combination of several factors, i.e. the different adsorption mode of the sulfur molecules and their different reaction mechanisms on one hand and the change in the catalyst characteristics such as the number and/or modification of the electronic properties of their active sites on the other hand. Indeed, while the smaller 3MT molecule, which adsorbs vertically over the catalysts and reacts with both S-edge and M-edge, could take advantage of all the active sites of the catalysts, the bigger BT molecule, which mainly reacts with M-edge and shows a flat adsorption by the benzenic ring, had more limited access to the active sites in these bulk catalysts due to steric hindrance. As a result, the transformation of 3MT alone was strongly affected by the change in properties of the catalysts with a clear advantage to NiMoS-NG. So, this investigation clearly shows that an effective transformation of sulfur model molecules representative of those present in FCC gasoline strongly relies on a good match between the properties of the catalyst (number and quality of active sites, accessibility) and the properties of the sulfur molecule involved (adsorption mode and transformation mechanism).

Acknowledgements

The authors thank the French "Agence Nationale de la Recherche" (ANR) for research project grant (ANR PASSCATA - ANR-16-CE07-0029).

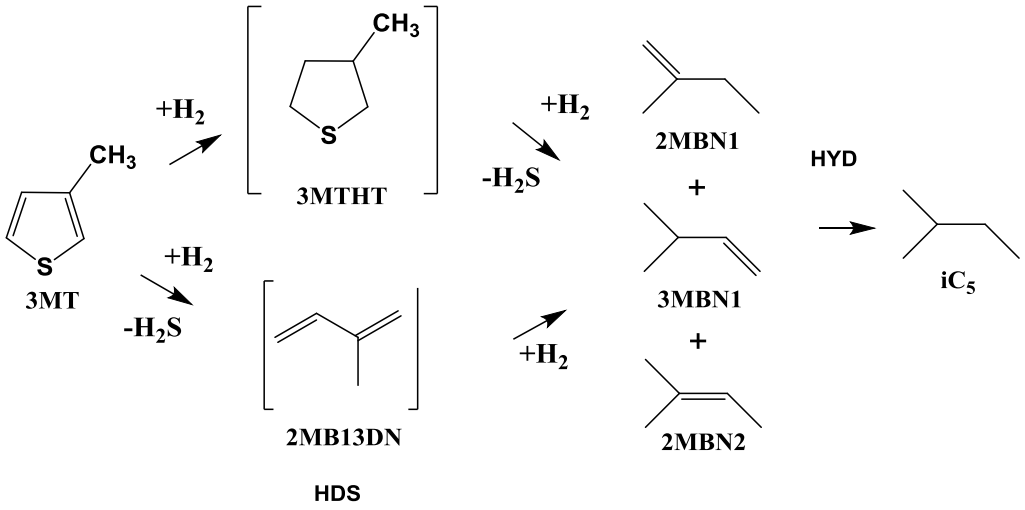

Scheme 1**:**. Transformation of 3-methylthiophene (3MT). (3-methyltetrahydrothiophene (3MTHT), 2-methyl-but-1-ene (2MBN1), 2-methyl-but-2-ene (2MBN2), 3MBN1 (3-methyl-but-1-ene), isopentane (iC_5), 2-methyl-but-1,3-diene (2MB13DN)

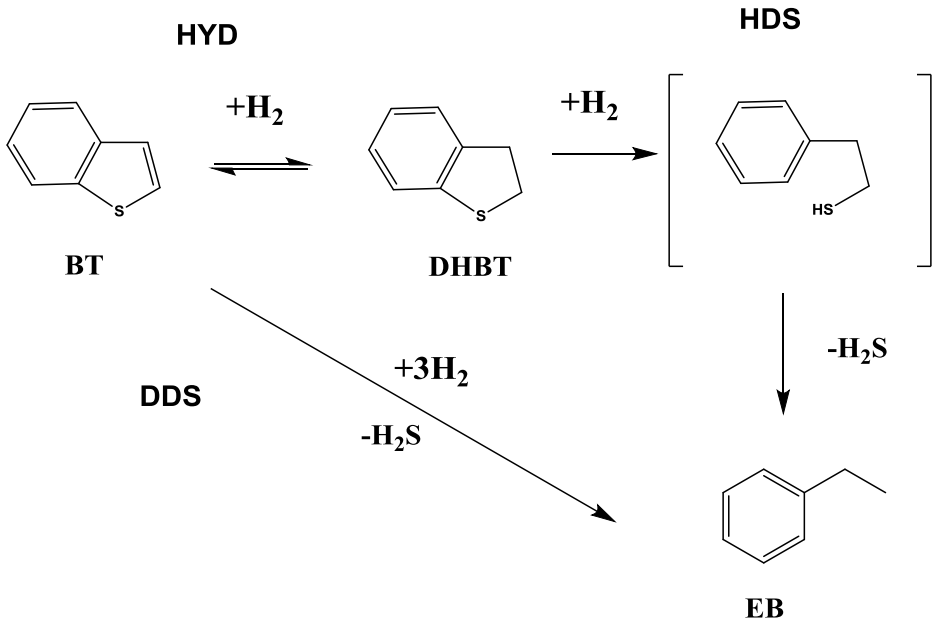

Scheme 2: Transformation of benzothiophene (BT): Dihydrobenzothiophene (DHBT), Ethylbenzene (EB).

Table 1: Partial pressure (kPa) of the different compounds for the sulfidation step and the transformation of the different feeds.

Pressure (kPa)	**Sulfidation**	**3MT (or BT)**
P_{H2S}	10	0
$P_{3MT\ \textbf{(or BT)}}$	0	2
P_{H2}	90	1366
P_{nC7}	0	632
Ptotal	100	2000

Table 2: Specific surface area (S_{BET}), elemental analysis of sulfur (S), nickel (Ni) and molybdenum (Mo) for NiMoS catalysts. Impact of synthesis methods (metathesis, M, and nucleation growth, NG).

Sample	S_{BET} ($m^2 \cdot g$)	S (wt.%)	Ni (wt. %)	Mo (wt.%)	Ni/(Ni+Mo) (molar)
M	31	34.6	17.6	34.6	0.45
NG	41	26.4	8.9	34.0	0.3

Table 3: XRD and TEM characterizations of NiMoS bulk catalysts. Impact of synthesis methods (metathesis, M, and nucleation growth, NG). MoS_2 particle size determined by XRD, stacking of MoS_2 layers determined from TEM images, average, minimal and maximal lengths of the layers determined by TEM with the standard deviation and dispersion, i.e. fraction of $Mo_{edges+corner}$ (D).

Catalyst	XRD	TEM					
	S [a] (nm)	St [b]	L [c] (nm)	σ^2 (nm)	Lmin (nm)	Lmax (nm)	D (%)
M	3.3	4.3	3.7	1.7	0.9	11.5	25
NG	2.6	4.1	2.5	1.0	0.8	7.0	36

[a] MoS_2 particle size (S), [b] average stacking (St), [c] average length (L), D (dispersion) : $D = \frac{\text{Mo edges+corner}}{\text{Mo total}} = \frac{\sum_i 6n_i - 6}{\sum_i 3n_i^2 - 3n_i + 1}$ with n_i : number of Mo atoms along one side of a MoS_2 slab determined from its length and i being the total number of slabs measured by TEM [39].

Table 4**:** S/Mo, Ni/Ni+Mo atomic ratios, MoS_2, NiS and NiO % amount determined by XPS for NiMoS bulk catalysts after sulfidation step. Impact of synthesis methods (metathesis, M, and nucleation growth, NG).

Catalyst	S/Mo (atom.)	MoS_2 (%)	NiMoS (%)	NiS (%)	NiO (%)	Ni/(Ni+Mo) (atom.)
M	2.3	80	57	28	15	0.39
NG	2.1	82	80	9	11	0.29

Table 5: 3MT transformation over NiMoS catalysts (M: metathesis, NG: nucleation growth): activity, adsorption constant (K) and kinetic constant (k).

Synthesis Method		M	NG
Activity	mmol/g h	2.2± 0.1	4.1± 0.2
	10^{-21} mol/at_{Mo}.h	4.1± 0.2	5.3± 0.2
Adsorption constant (K: bar^{-1})	K_{3MT}	5.5 ± 0.2	8.0 ± 0.2
Kinetic constant (k: h^{-1})	k_{HDS}	(1.4 ± 0.1) 10^{12}	(2.6 ± 0.1) 10^{12}
	k_{HYD}	(1.3 ± 0.1) 10^{12}	(1.0 ± 0.1) 10^{12}

Table 6**:** Transformation of BT over NiMoS bulk catalysts (M: metathesis, NG: Nucleation Growth) on activity, adsorption constant (K) and kinetic constant (k).

Synthesis method		M	NG
Activity	mmol/g h	4.2± 0.2	4.5± 0.2
	10^{-21} mol/at_{Mo}.h.	7.7± 0.3	5.9± 0.2
Adsorption constant (K: bar^{-1})	K_{BT}	7.4 ± 0.2	8.2 ± 0.2
Kinetic constant (k: h^{-1})	k_{HYD}	(2.0 ± 0.1) 10^{12}	(5.3 ± 0.2) 10^{12}
	k_{HDS}	(2.0 ± 0.2) 10^{13}	(2.6 ± 0.2) 10^{13}
	k_{DDS}	(3.5 ± 0.2) 10^{12}	(6.4 ± 0.2) 10^{12}

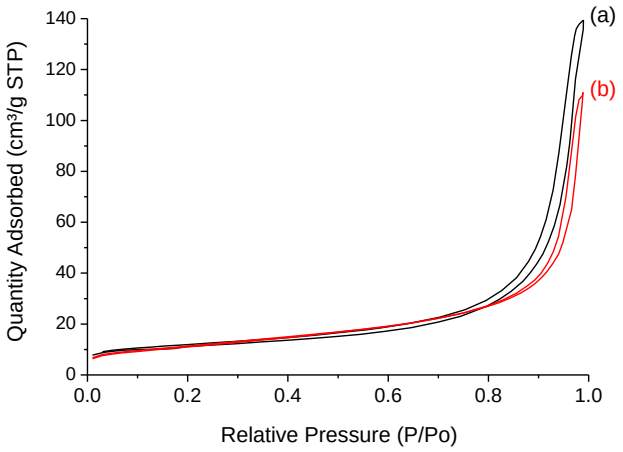

Figure 1: Nitrogen adsorption–desorption analysis for NiMoS bulk catalysts prepared (a) by metathesis (M) and (b) by nucleation growth (NG)

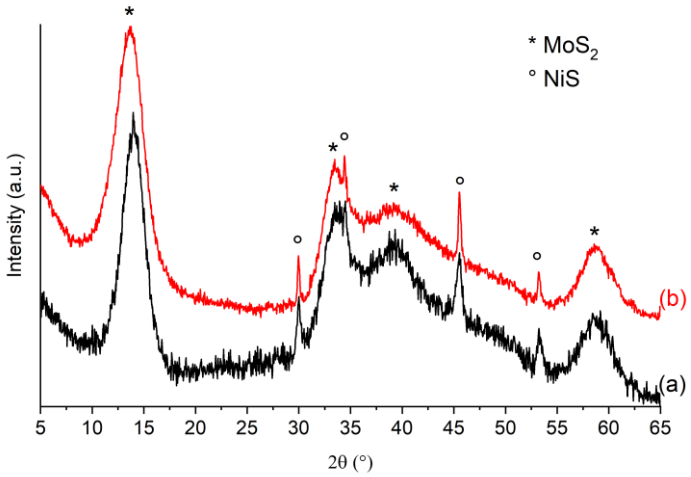

Figure 2: X-ray diffractograms of catalysts prepared (a) by Metathesis (M) and (b) by Nucleation Growth (NG).

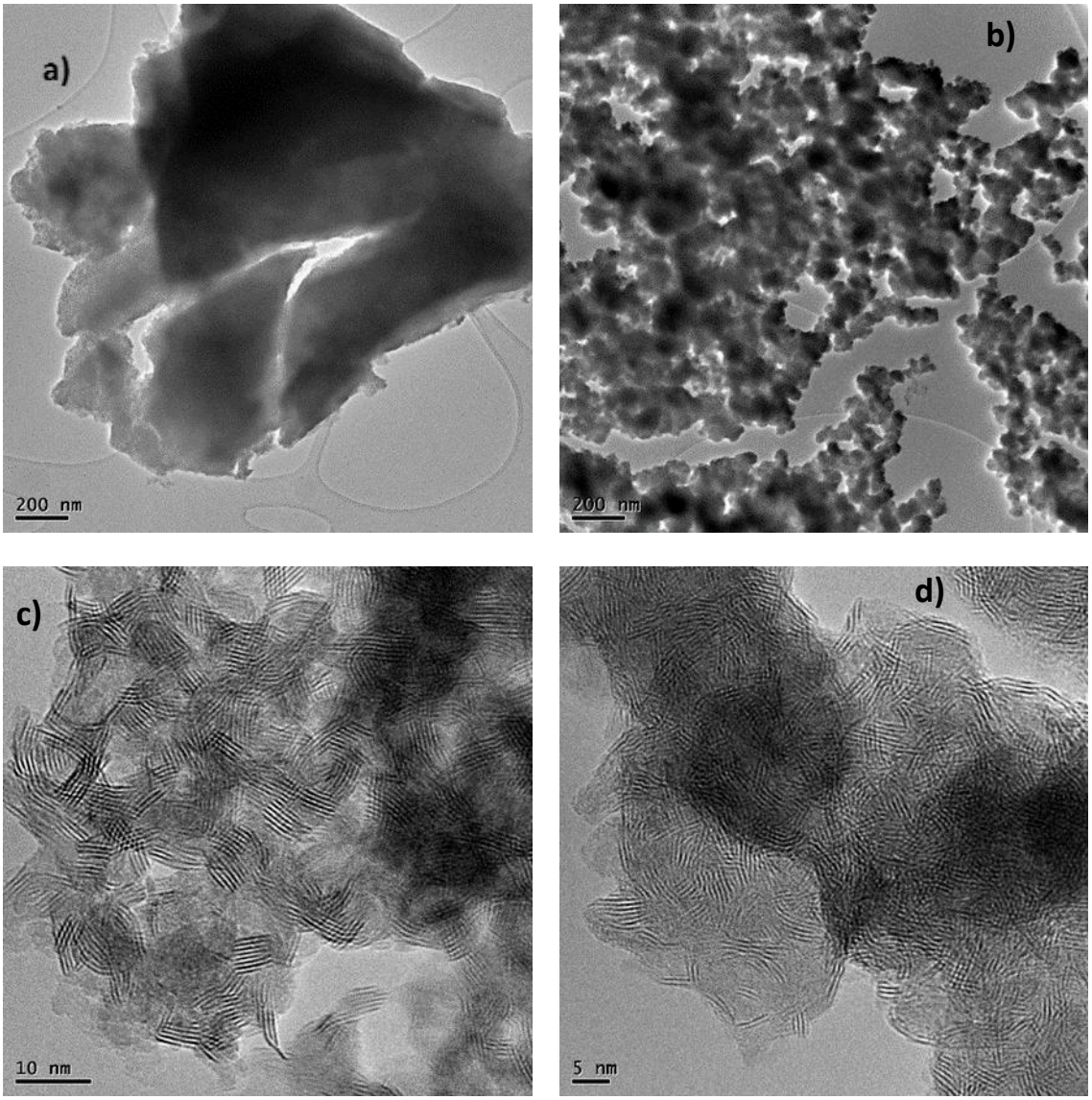

Figure 3: TEM images of NiMoS bulk catalysts prepared (a) and (c) by metathesis (M) and (b) and (d) by nucleation growth (NG).

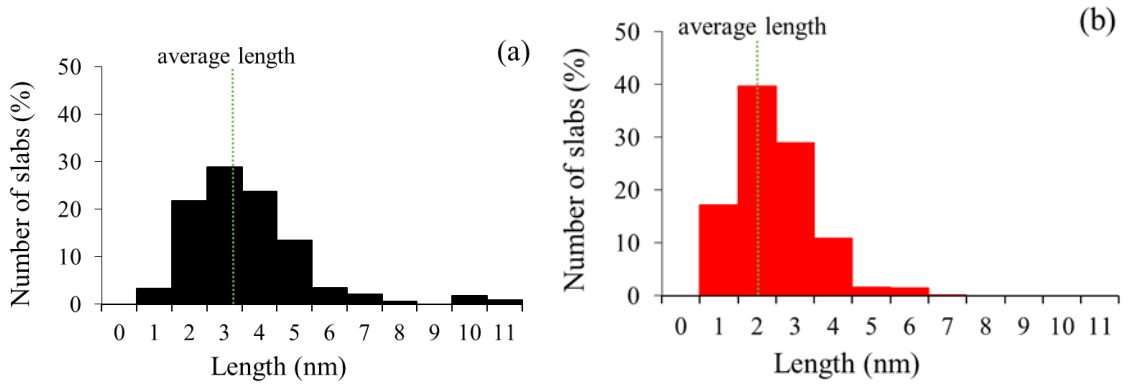

Figure 4: Histograms of the slab distribution as a function of their length determined from TEM images for NiMoS bulk samples prepared by a) metathesis (M) and b) nucleation growth (NG), (analysis based on 400 particles).

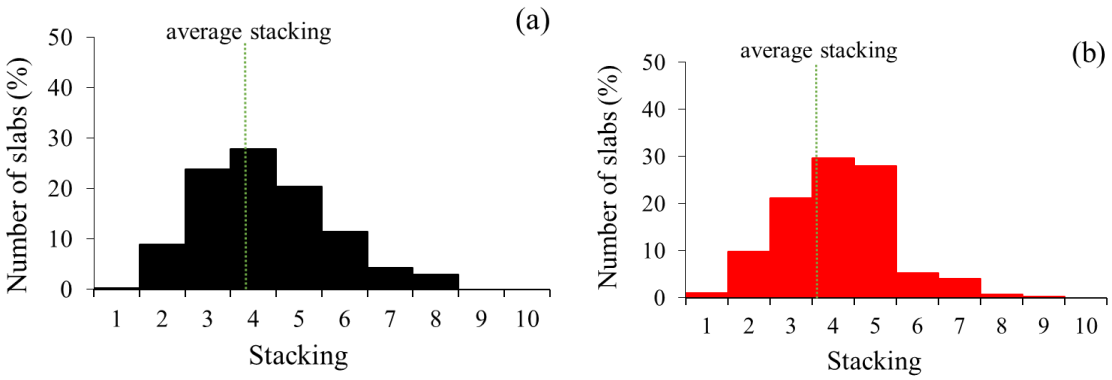

Figure 5: Histograms of the slab distribution as a function of their stacking determined from TEM images for NiMoS bulk samples prepared by a) metathesis (M) and b) nucleation growth (NG), (analysis based on 400 particles).

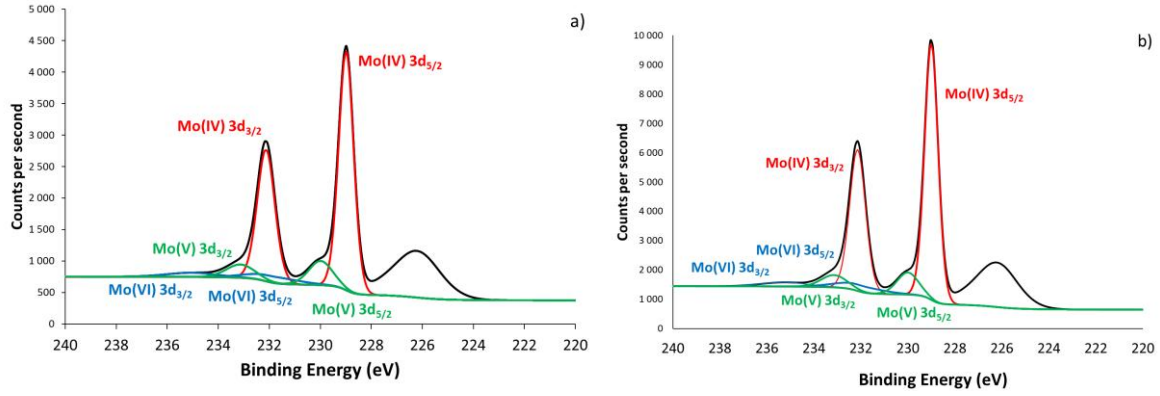

Figure 6: XPS spectra of molybdenum element (Mo3d) of NiMoS catalysts prepared by (a) Metathesis (M) and (b) Nucleation Growth NG

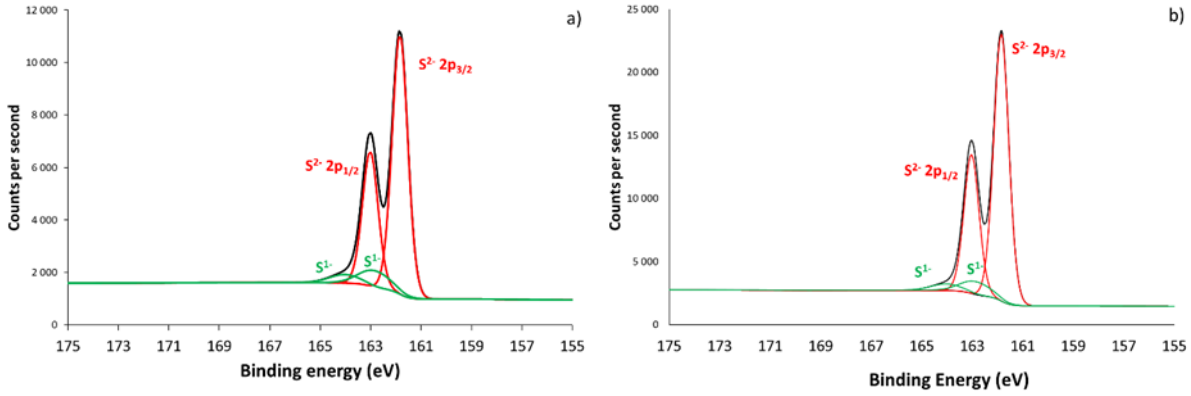

Figure 7: XPS spectra of sulfur element (S2p) of NiMoS catalysts prepared by (a) Metathesis (M) and (b) Nucleation Growth NG

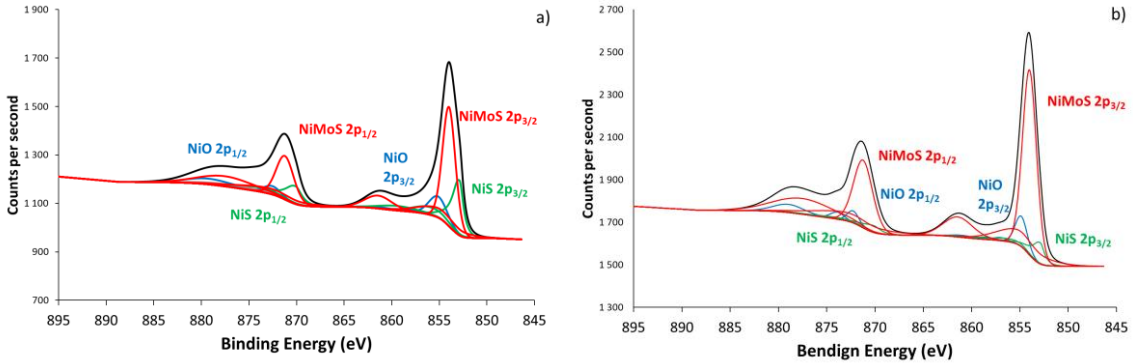

Figure 8**:** XPS spectra of nickel element (Ni2p) of NiMoS catalysts prepared by (a) Metathesis (M) and (b) Nucleation Growth NG.

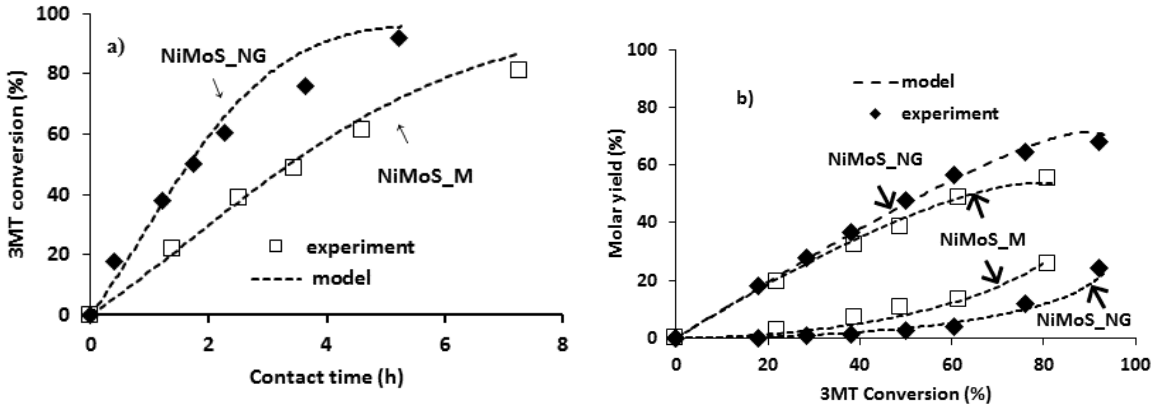

Figure 9: 3MT transformation over NiMoS catalysts (M: metathesis, NG: nucleation growth). (a) conversion and (b) product distribution as function of contact time or 3MT conversion. Comparison of simulation results (dotted lines) and experimental data (points). (T = 250 °C, P = 2.0 MPa, H_2/feed = 360 N L/L).

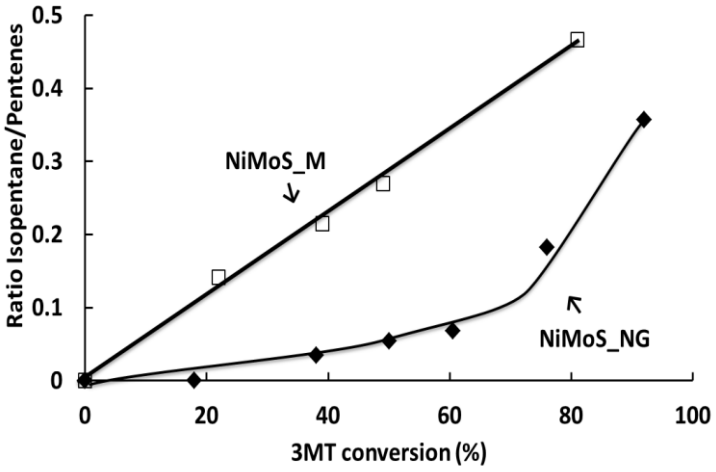

Figure 10: 3MT transformation over NiMoS catalysts (M: metathesis, NG: nucleation growth). Isopentane/pentene ratio as a function of 3MT conversion (T = 250 °C, P = 2.0 MPa, H_2/feed = 360 N L/L).

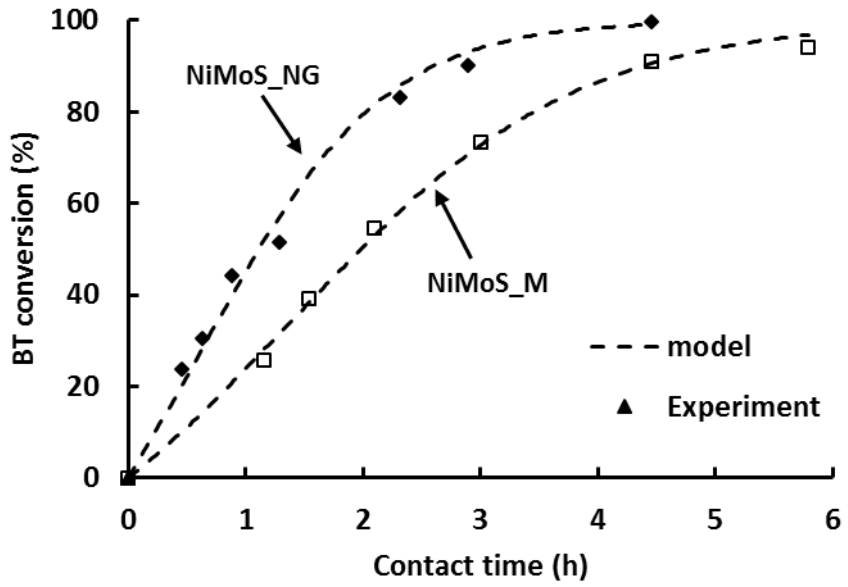

Figure 11: BT transformation over NiMoS catalysts (M: metathesis, NG: nucleation growth) as function of contact time. Comparison of simulation results (dotted lines) and experimental data (points). (T = 250 °C, P = 2.0 MPa, H_2/feed = 360 N L/L).

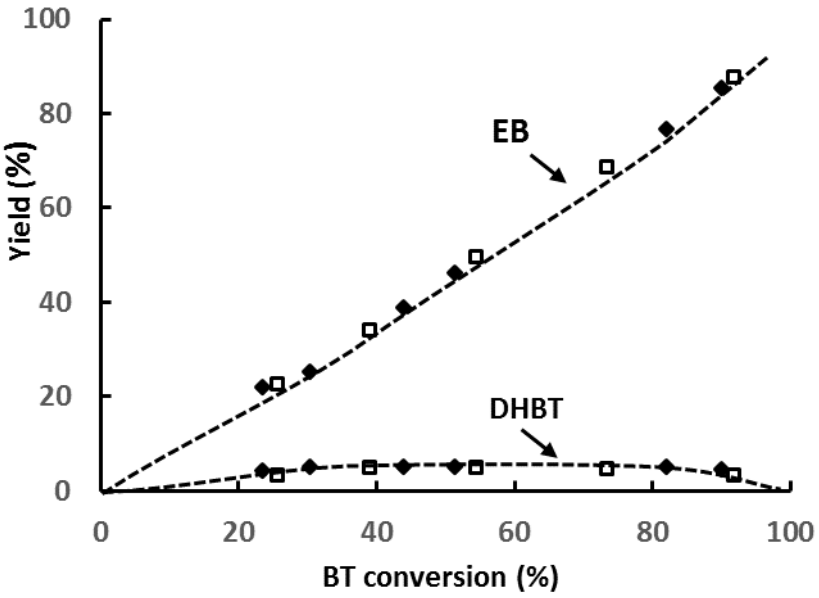

Figure 12: BT transformation over NiMoS catalysts (M: metathesis (Full symbol), NG: nucleation growth (Empty symbol)). Product distribution as function of BT conversion. Comparison of simulation results (dotted lines) and experimental data (points). (T = 250 °C, P = 2.0 MPa, H_2/feed = 360 N L/L). (EB: Ethylbenzene, DHBT: Dihydrobenzothiophene)

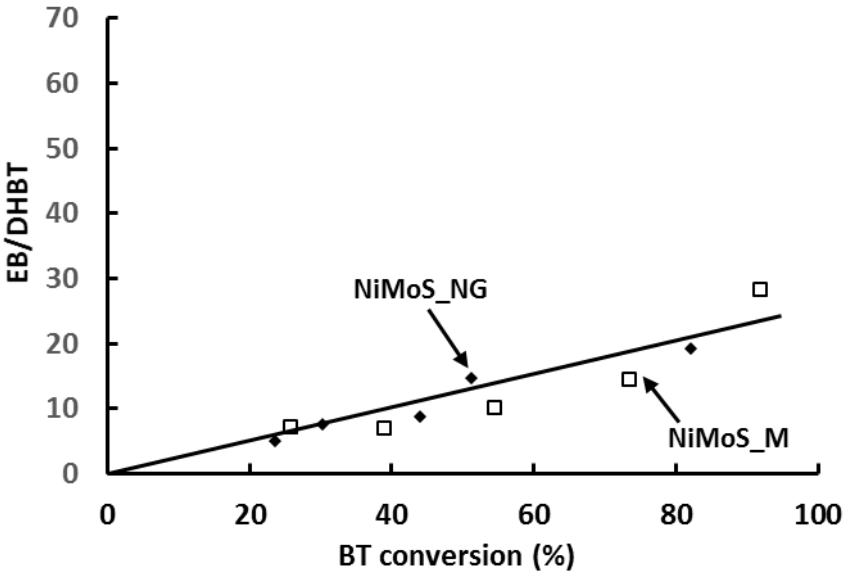

Figure 13: BT transformation over NiMoS catalysts (M: metathesis, NG: nucleation growth). EB/DHBT ratio as function of BT conversion (T = 250 °C, P = 2.0 MPa, H_2/feed = 360 N L/L). (EB: Ethylbenzene, DHBT: Dihydrobenzothiophene).

Reference

[1] Transport Policy: information on energy and environmental regulations in the transportation sector.

http://transportpolicy.net/index.php?title=Global_Comparison:_Fuels (accessed 14 September 2022).

[2] P. Afanasiev, C. R. Chimie 11 (2008) 159-182.

[3] J. V. Lauritsen, J. Kibsgaard, G. H. Olesen, P. G. Moses, B. Hinnemann, S. Helveg , J. K. Nørskov, B. S. Clausen, H. Topsøe, E. Lægsgaard, F. Besenbacher, J. Catal. 249 (2007) 220–233.

[4] J V Lauritsen, M Nyberg, R T Vang, M V Bollinger, B S Clausen, H Topsøe, K W Jacobsen, E Lægsgaard, J K Nørskov, F Besenbacher, Nanotechnol. 14 (2003) 385–389.

[5] A.S. Walton, J.V. Lauritsen, H. Topsøe, F. Besenbacher, J. Catal. 308 (2013) 306–318.

[6] T. Chapuis, D. Hudebine, V. Souchon**,** Catalysis by transition metal sulfides: from molecular theory to industrial application, IFPEN-Lyon, Technip Edition, Paris, 2013 pp. 547-578.

[7] Y. Sun, H. Wang, R. Prins, Catal. Today, 150 (2010) 213–217.

[8] H. Toulhoat and P. Raybaud, Catalysis by transition metal sulphides. From molecular theory to industrial application, Technip, Paris, France, 2013.

[9] A. Stanislaus, A. Marafi and M. S. Rana, Catal Today 153 (2010) 1-68.

[10] S. Brunet, D. Mey, G. Pérot, C. Bouchy and F. Diehl, Appl Catal. A: Gen. 278 (2005) 143-172.

[11] M. Breysse, C. Geantet, P. Afanasiev, J. Blanchard and M. Vrinat, Catal. Today 130 (2008) 3-13.

[12] A. Tanimu, K. Alhooshani, Energy Fuels 33 (2019) 2810−2838.

[13] L. Alvarez, J. Espino, C. Ornelas, J.L. Rico, M.T. Cortez, G. Berhault, G. Alonso. J. Mol. Catal. A Chemical 210 (2004) 105-117.

[14] H. Liu, C. Yin, B. Liu. X. Li, Y. Li, Y. Chai, C. Liu. Energy & Fuels 28 (2014) 2429-2436.

[15] H. Liu, C. Liu, C. Yin, Y. Chai, Y. Li, D. Liu, B. Liu. X. Li, Y. Wang, X. Li. Appl. Catal. B: Environ. 174-175 (2015) 264-276.

[16] W. Song, W. Lai, Z. Chen, J. Cao, H. Wang, Y. Lian, W. Yang, X. Jiang. ACS Appl. Nano Mater. 1 (2018) 442−454.

[17] H. Liu, C. Yin, X. Li, Y. Chai, Y. Li, C. Liu, Catal. Today 282 (2017) 222–229.

[18] S. Fuentes, G. Diaz, F. Pedraza, H. Rojas, N. Rosas. J. Catal. 113 (1988) 535-539.

[19] W. Lai, Z. Chen, J. Zhu, L. Yang, J. Zheng, X. Yi, W. Fang. Nanoscale. 8 (2016) 3823-3833.

[20] A.-F. Lamic, A. Daudin, S. Brunet, C. Legens, C. Bouchy, E. Devers. Appl. Catal. A: Gen. 344 (2008) 198–204.

[21] C. Fontaine, Y. Romero, A. Daudin, E. Devers, C. Bouchy, S. Brunet, Appl. Catal. A: Gen. 388 (2010) 188–195.

[22] E. Devers, P. Afanasiev, B. Jouguet, M. Vrinat, Catal. Letters 82(1-2) (2002) 13–17.

[23] K. Sun, H. Guo, F. Jiao, Y. Chai, Y. Li, B. Liu, S. Mintova, C. Liu, Appl. Catal. B: Environ. 286 (2021) 119907-119907

[24] D. Ryaboshapka, L. Piccolo, M. Aouine, P. Bargiela, V. Briois, P. Afanasiev, Appl. Catal. B: Environ. 302 (2022) 120831-120842

[25] J. A. Medina Cervantes, R. Huirache-Acuña, J. N. Díaz de León, S. Fuentes Moyado, J. Cruz-Reyes, G. Alonso-Núñez, Reac. Kinet. Mech. Cat. 131 (2020) 187–198.

[26] L. B. Romero-Sánchez, G. Alonso-Núñez, R. Prieto-García, J. N. Díaz de León, S. Fuentes, M. Del Valle, K. Vega-Granados, F. Paraguay-Delgado, J. Cruz-Reyes, Reac. Kinet. Mech. Cat. 133 (2021) 1027–1044.

[27] M. H. Siadati, G. Alonso, B. Torres, R.R. Chianelli, Appl. Catal. A: Gen. 305 (2006) 160–168.

[28] D. Genuit, P. Afanasiev, M. Vrinat, J. Catal. 235(2) (2005**)** 302–317.

[29] V. Hetier, D. Peña, A. Carvalho, L. Courthéoux, V. Flaud, E. Girard, D. Uzio, S. Brunet, P. Lacroix-Desmazes, A. Pradel. Catalysts 9 (2019) 793:1-17.

[30] I. Bezverkhy, P. Afanasiev, M. Lacroix, Inorg. Chem. 39 (2000) 5416-5417.

[31] A. Dos Santos, E.Girard, P.Leflaive, S. Brunet. Appl. Catal. A: Gen. 570 (2019) 292-298.

[32] J. McDonald, G. Friesen, L. Rosenhein, W. Newton, Inorganica Chimica Acta, 72 (1983) 205-210.

[33] P. Afanasiev, G.F. Xia, G. Berhault, B. Jouguet, M. Lacroix, Chem. Mater. 11 (1999) 3216-3219.

[34] L. Coulier, V.H.J. de Beer, J.A.R. van Veen, J.W. Niemantsverdriet, J. Catal. (2001) 26-33.

[35] A.D. Gandubert, C. Legens, D. Guillaume, S. Rebours, E. Payen, Oil Gas Sci. Technol. 62 (2007) 79-89.

[36] D. Mey, S. Brunet, C. Canaff, F. Maugé, C. Bouchy, F. Diehl, J. Catal. 227 (2004) 436-447.

[37] A. Daudin, S. Brunet, G. Perot, P. Raybaud, C. Bouchy, J. Catal. 248 (2007) 111-119.

[38] F. Pelardy, A. Silva dos Santos, A. Daudin, E. Devers, T. Belin, S. Brunet, Appl. Catal. B: Environ. 206 (2017) 24–34.

[39] S. Ghosh, L. Courthéoux, S. Brunet, P. Lacroix-Desmazes, A. Pradel, E. Girard, D. Uzio. Appl. Catal. A: Gen. 623 (2021) 118264-118273.

[40] H. Liu, Q. Liu, J. Zhang, C. Yin, Y. Zhao, S. Yin, C. Liu, W. Suna, Fuel Process. Technol. 160 (2017) 93-101.

[41] G. Leyral, S. Brillouet, J. Rousseau, F. Richard, A.S. Mamede, L. Courtheoux, A. Pradel, M. Ribes, S. Brunet, Appl. Catal. A: Gen. 532 (2017) 120-132.

[42] J. Xu, C. Shi, Z. Xiao, R. Gao, Y. Li, X. Zhang, L. Pan, J.J. Zou, Chem. Com.. 56 (2020) 5540-5543.

[43] S. Hatanaka, E. Morita, K. Shimada, J. Jpn. Pet. Inst. 50 (2007) 179–185.

[44] S. Hatanaka, M. Yamada, Ind. Eng. Chem. Res. 36 (1997) 1519–1523.

[45] J.M.J.G. Lipsch, G.C.A. Schuit, J. Catal. 15-2 (1969) 179-189.

[46] S. Kolboe, Can. J. Chem. 47-2 (1969) 352-355.

[47] H. Wang, R. Prins, Appl. Catal. A: Gen. 350 (2008) 191–196.